In vitro and *in vivo* targeting of hollow gold nanoshells directed at epidermal growth factor receptor for photothermal ablation therapy

Marites P. Melancon,[1] Wei Lu,[1] Zhi Yang,[1] Rui Zhang,[1] Zhi Cheng,[1] Andrew M. Elliot,[2] Jason Stafford,[2] Tammy Olson,[3] Jin Z. Zhang,[3] and Chun Li[1]

Departments of [1]Experimental Diagnostic Imaging and [2]Imaging Physics, The University of Texas M. D. Anderson Cancer Center, Houston, Texas and [3]Department of Chemistry and Biochemistry, University of California, Santa Cruz, California

Abstract

Laser-induced phototherapy is a new therapeutic use of electromagnetic radiation for cancer treatment. The use of targeted plasmonic gold nanoparticles can reduce the laser energy necessary for selective tumor cell destruction. However, the ability for targeted delivery of the currently used gold nanoparticles to tumor cells is limited. Here, we describe a new class of molecular specific photothermal coupling agents based on hollow gold nanoshells (HAuNS; average diameter, ~30 nm) covalently attached to monoclonal antibody directed at epidermal growth factor receptor (EGFR). The resulting anti-EGFR-HAuNS exhibited excellent colloidal stability and efficient photothermal effect in the near-infrared region. EGFR-mediated selective uptake of anti-EGFR-HAuNS in EGFR-positive A431 tumor cells but not IgG-HAuNS control was shown *in vitro* by imaging scattered light from the nanoshells. Irradiation of A431 cells treated with anti-EGFR-HAuNS with near-infrared laser resulted in selective destruction of these cells. In contrast, cells treated with anti-EGFR-HAuNS alone, laser alone, or IgG-HAuNS plus laser did not show observable effect on cell viability. Using ^{111}In-labeled HAuNS, we showed that anti-EGFR-HAuNS could be delivered to EGFR-positive tumors at 6.8% ID/g, and the microscopic image of excised tumor with scattering signal from nanoshells confirmed preferential delivery to A431 tumor of anti-EGFR-HAuNS compared with IgG-HAuNS. The absence of silica core, the relatively small particle size and high tumor uptake, and the absence of cytotoxic surfactant required to stabilize other gold nanoparticles suggest that immuno-HAuNS have the potential to extend to *in vivo* molecular therapy. [Mol Cancer Ther 2008;7(6):1730–9]

Introduction

Phototherapy is a new therapeutic use of electromagnetic radiation for treating various medical conditions, including cancer (1). This type of cancer therapy is gaining increasing popularity, because specific amount of energy is delivered directly into the tumor mass. The laser energy delivered to the targeted tumors can induce localized photochemical, photomechanical, and photothermal reactions that kill the tumor cells (2). In photochemical reactions (that is, photodynamic therapy), toxic free radicals such as singlet oxygen are formed, leading to the death of target tissues. Photomechanical reactions may induce cell stress by means of mechanical force, including the generation and collapsing of bubbles inside cells, resulting in cellular disruption (3). Photothermal reactions (that is, photothermal ablation) uses heat generated through absorption of light to directly destroy tissue. Photothermal ablation as a minimally invasive treatment has been used successfully for ablation of tumors throughout the body, especially liver lesions (1, 4). However, this therapy approach, like other thermal delivery methods, such as radiofrequency (5), microwave (6), and focused ultrasound ablation therapies (7, 8), is limited by the same fact that the heating from these energy sources is nonspecific. Treatment volume and speed are therefore limited by potential damage of the surrounding normal tissues.

The efficiency of photothermal ablation can be significantly enhanced when a light-absorbing material is applied to the target tissue to mediate selective photothermal effects (9, 10). Noble metal nanoparticles exhibit a strong optical extinction at visible and near-infrared (NIR) wavelengths due to a localized surface plasma resonance of their free electrons on excitation by an electromagnetic field. Gold nanoshells (AuNS), composed of metallic gold and a dielectric core such as silica, have a cross-section absorption that is ~1 million-fold greater than that of conventional NIR dye indocyanine green (10). These nanoparticles can be fabricated with a defined core-shell ratio to absorb NIR light (wavelength, 700-850 nm), resulting in resonance and transfer of thermal energies to the surrounding tissue. The absorption band in the NIR region is a desirable property,

Received 1/7/08; revised 2/28/08; accepted 3/30/08.

Grant support: NIH grant R01 CA119387, John S. Dunn Foundation (C. Li), and Department of Defense (J.Z. Zhang).

Note: Z. Yang is on leave from the Department of Nuclear Medicine, Peking University School of Oncology and Beijing Cancer Hospital, Beijing, People's Republic of China 100036.

The costs of publication of this article were defrayed in part by the payment of page charges. This article must therefore be hereby marked *advertisement* in accordance with 18 U.S.C. Section 1734 solely to indicate this fact.

Requests for reprints: Chun Li, Department of Experimental Diagnostic Imaging, The University of Texas M. D. Anderson Cancer Center, Unit 59, 1515 Holcombe Boulevard, Houston, TX 77030. Phone: 713-792-5182; Fax: 713-794-5456. E-mail: cli@di.mdacc.tmc.edu

doi:10.1158/1535-7163.MCT-08-0016

because normal tissues are relatively transparent to NIR light; thus, irradiation with NIR light causes minimal thermal injury to normal tissues (11). O'Neal et al. (12) reported AuNS-induced photothermal ablation in a s.c. murine colon tumor model after i.v. injection of the nanoshells. These polyethylene glycol–coated AuNS (~130 nm in diameter) accumulated in the tumor passively because of the enhanced permeability and retention effect, by which nanoscale materials are preferentially deposited in tumors (as opposed to normal tissue) due to the leaky nature of tumor vessels (13). Active targeting, on the other hand, may enhance *in vivo* delivery of AuNS by facilitating extravasation from tumor blood vessels as well as extravascular transport through the interaction between tumor cell surface receptors and receptor ligands attached to AuNS. Selective ablation of tumor cells has been shown *in vitro* using various shapes of immuno-gold nanoparticles, including spherical AuNS (14) and gold nanocage (15) targeted to HER-2/*neu* receptors and gold nanorods targeted to EGFR (16, 17). However, active targeting of gold nanoparticles capable of mediating photothermal effect *in vivo* has not yet been shown.

In the present work, we report the use of hollow AuNS (HAuNS), which have an average diameter of ~30 nm, as a new class of potential photothermal therapeutic agents. HAuNS were composed only of a thin gold wall with a hollow interior and displayed a strong resonance absorption peak tunable in the NIR region (18). We have developed a covalent conjugation method to enable the synthesis of monoclonal antibody-conjugated HAuNS with excellent colloidal stability. We show both the selective destruction of epidermal growth factor receptor (EGFR)–positive cancer cells *in vitro* and the enhanced delivery to EGFR-positive tumors *in vivo* using anti-EGFR monoclonal antibody conjugated HAuNS. EGFR is a transmembrane glycoprotein with an intracellular tyrosine kinase domain. EGFR and its ligands, including EGF, are frequently overexpressed in a variety of solid tumors including cancers of the brain, breast, colon, head and neck, lung, ovary, and pancreas (19–21).

Materials and Methods

Materials

Monoclonal anti-EGFR antibody C225 was obtained from ImClone Systems. C225 is a chimeric human-mouse IgG1 that binds EGFR with high affinity (22, 23). Methoxy-polyethylene glycol-SH (molecular weight, 5,000) was obtained from Nektar. *N*-succinimidyl *S*-acetylthioacetate and PBS (pH 7.4) were purchased from Sigma. *p*-Isothiocyanatobenzyl-diethylenetriaminepentaacetic acid was obtained from Macrocyclics. Trisodium citrate dihydrate (>99%), cobalt chloride hexahydrate (99.99%), sodium borohydride (99%), and chloroauric acid trihydrate (ACS reagent grade) were purchased from Fisher and used as received. Mouse IgG and viability/cytotoxicity staining kit, including calcein AM and ethidium homodimer-1 (EthD-1), were purchased from Invitrogen. ^{111}In radionuclide was obtained from Perkin-Elmer.

Synthesis of HAuNS

HAuNS were synthesized according to the method of Schwartzberg et al. (18). Briefly, cobalt nanoparticles were first synthesized by deoxygenating 100 mL deionized water containing 400 μL of 0.1 mol/L sodium citrate and 100 μL of 0.4 mol/L cobalt chloride by bubbling the solution with nitrogen (~20-30 min). Sodium borohydride (100 μL, 1 mol/L) was then added. The clear, slightly pinkish solution turned brown on the addition of sodium borohydride, indicating the reduction of Co(II) and the formation of cobalt nanoparticles. The solution was allowed to stand at room temperature for 45 min under constant nitrogen flow until the complete hydrolysis of the sodium borohydride. Thereafter, 30 mL of the cobalt nanoparticle solution were transferred immediately to a vortexing solution of 10 mL deionized water containing 15 to 35 μL of 0.1 mol/L chloroauric acid. The cobalt immediately reduced the gold ions onto the surface of cobalt nanoparticles while at the same time it was oxidized to cobalt oxide. Any remaining cobalt core was further oxidized by air, resulting in the final product, HAuNS.

Synthesis of C225-DTPA-ATA and IgG-DTPA-ATA

An aqueous solution of C225 (2.5 mg, 0.017 μmol; 5 mg/mL) was first allowed to react with *N*-succinimidyl *S*-acetylthioacetate (0.077 mg, 0.332 μmol) at room temperature for 1 h. The resulting conjugate, C225-acetylthioacetate (C225-ATA), was purified by passing through a gel filtration PD-10 column (Amersham Pharmacia) using Protein Dye kit (Bio-Rad) as an indicator to guide the collection of antibody-containing fractions. The purified C225-ATA was then reacted with *p*-isothiocyanatobenzyl-diethylenetriaminepentaacetic acid (0.216 mg, 0.332 μmol) at 4°C overnight in aqueous solution in which the pH value was adjusted to 8 using 0.1 mol/L $NaHCO_3$. The product was purified by passing through a PD-10 column to remove excess *p*-isothiocyanatobenzyl-diethylenetriaminepentaacetic acid to yield DTPA-C225-ATA.

The same procedures were used for the synthesis of DTPA-IgG-ATA.

Conjugation of Antibodies to the HAuNS

Before conjugation to HAuNS, aliquots of aqueous solution of DTPA-C225-ATA or DTPA-IgG-ATA (0.5 mL, 20 μg/mL) were treated with hydroxylamine (50 mmol/L, 50 μL) at room temperature for 2 h to expose free SH. After passing through PD-10 column, the resulting DTPA-C225-SH or DTPA-IgG-SH was added to aqueous solution of HAuNS (7.3×10^{10} particles/mL) to a final antibody concentration of 5 μg/mL. The suspension was stirred at room temperature for 1 h. Thereafter, polyethylene glycol-SH was added to the antibody-coated HAuNS to a final concentration of 0.2 mg/mL and the mixture was reacted for an additional 1 h to ensure that the gold surface was completely covered. DTPA-C225-HAuNS and DTPA-IgG-HAuNS were centrifuged at 8,000 rpm for 5 min, and the resulting pellet was washed twice with deionized water. The presence of free C225 in the supernatant was examined with the Bio-Rad protein dye. No free C225 was detected in the supernatant after the second wash. The purified

products were resuspended in 0.1 mmol/L PBS and stored at 4°C until further use. Antibody-conjugated HAuNS were stable in physiologic buffers for at least 3 weeks at 4°C without aggregation.

Characterization of Nanoparticles

For transmission electron microscopic (TEM) study, plain HAuNS and DTPA-C225-HAuNS were applied onto a 100-mesh, formvar- and carbon-coated nickel grid. The nanoparticles were allowed to adhere on the grid for 1 h, after which they were briefly rinsed with deionized water and air dried. The samples were then examined using a JEOL TEM at an accelerating voltage of 80 kV. The average nanoshell diameter and thickness of the shell were determined by measuring up to 45 individual HAuNS particles. The particle size was also determined using dynamic light scattering at a scatter angle of 90° on a Brookhaven particle size analyzer. UV-visible spectroscopy was recorded on a Beckman Coulter UV-visible spectrometer. The concentration of gold atoms of a HAuNS solution was analyzed by inductively coupled plasma mass spectroscopy (Galbraith).

Quantification of the Number of Antibodies per HAuNS Particle

The concentration of antibody was estimated using the bicinchoninic acid protein assay according to manufacturer's protocol (Pierce). Aliquots containing C225 antibody (concentration range, 0.5-20 μg/mL) were used as standards. Absorbance values were measured at 562 nm with a Molecular Devices spectrophotometer. The absorbance value of antibody-coated HAuNS was subtracted from the absorbance measured for plain HAuNS of equal particle concentration to correct for HAuNS background. The concentration of antibody in solution of C225-HAuNS was extrapolated from the linear curve from the C225 standard. The number of C225 on each HAuNS was calculated by dividing the concentration of C225 by the concentration of the nanoshells.

Cell Culture and *In vitro* Cell Binding

Human squamous carcinoma A431 cells overexpressing EGFR were first seeded onto a 96-well plate (10,000 per well). The next day, cells were washed three times with HBSS and incubated with C225-HAuNS (100 μL, 7.3×10^{10} particles/mL), IgG-HAuNS (100 μL, 7.3×10^{10} particles/mL), or C225-HAuNS plus C225 (500 μg/mL) at 37°C for 30 min. Thereafter, the cells were washed three times with HBSS and fixed with 70% ethanol. Cell nuclei were stained with 4,6-diamidino-2-phenylindole (DAPI) for 5 min. Cells were then washed, mounted on slides, and examined using a Leica DML/HCS microscope. The AuNS was examined with a dark-field condenser illuminated by halogen light source, and the fluorescence of cell nuclei was detected with a Chroma DAPI filter illuminated by a Xenon XBO light source (OSRAM). The images were collected by using a Hamamatsu B/W chilled charge-coupled device camera (Hamamatsu) and processed by Image-Pro Plus 4.5.1 software (Media Cybernetics).

Photothermal Effect in HAuNS Solutions

The laser was a continuous wave GCSLX-05-1600m-1 fiber-coupled diode laser (China Daheng Group) with a center wavelength of 808 ± 10 nm. A 5-m, 600-μm core BioTex LCM-001 optical fiber was used to transfer laser light from the laser unit to the target. This fiber had a lens mounting at the output that allowed the laser spot size to be changed by changing the distance from the output to the target. The output power was independently calibrated using a handheld optical power meter (Newport model 840-C) and was found to be 1 W for a spot diameter of 3.5 mm (~8 W/cm^2) and a 2-amp supply current. For measuring temperature change mediated by HAuNS, NIR laser light (808 nm) was delivered through a quartz cuvette containing the nanoshells (100 μL). A thermocouple was inserted into the solution perpendicular to the path of the laser light. The temperature was measured over a period of 15 min. Water was used as a control.

In vitro Photothermal Ablation of Tumor Cells

A431 cells were seeded onto a 96-well plate with a density of 10,000 per well 1 day before the irradiation experiment. Cells were washed three times with HBSS. The following treatments were used: no treatment, NIR laser alone, C225-HAuNS alone, IgG-HAuNS plus NIR laser, and C225-HAuNS plus laser. For treatment with HAuNS, cells were incubated with HAuNS or C225-HAuNS (100 μL, 7.3×10^{10} particles/mL) at 37°C for 1 h. Thereafter, cells were washed three times with HBSS to remove unbound nanoshells. Cells were then resupplied with DMEM/F-12 containing 10% fetal bovine serum. Cells were irradiated with NIR laser light centered at 808 nm at an output power of 40 W/cm^2 for 5 min (Diomed) and then incubated at 37°C for 24 h. The diode laser was coupled to a 1-m, 2-mm core fiber, which delivered a circular laser beam of 2 mm in diameter, covering the central area of the microplate well. Power calibration was done automatically.

Twenty-four hours after laser treatment, cells were washed three times with HBSS and stained with calcein AM for visualization of live cells and with EthD-1 for visualization of dead cells. Cells were examined using an Olympus model IX81 laser scanning confocal microscope equipped with filter sets specific for excitation/emission wavelengths at 494/517 nm for calcein and 528/617 nm for EthD-1.

Radiolabeling

Aliquots of DTPA-C225-HAuNS or DTPA-IgG-HAuNS (7.3×10^{10} particles/mL, 0.1 mL) in 0.1 mol/L sodium acetate solution (pH 5.5) were mixed with an aqueous solution of $^{111}InCl_3$ (~200 μCi) for 30 min. The radiolabeled HAuNS was then purified by centrifugation at 4,000 rpm for 5 min and washed three times with PBS. Radiolabeled nanoshells were analyzed using instant TLC. The instant TLC strips were developed with PBS (pH 7.4) containing 4 mmol/L EDTA and quantified using a TLC Imaging Scanner (Bioscan). Free $^{111}In^{3+}$ moved to the solvent front (Rf = 0.9), and the nanoshells remained at the original spot (Rf = 0.0).

Biodistribution

All experiments involving animals were done in accordance with the guidelines of the Institutional Animal Care and Use Committee. A431 tumors were grown s.c. in the

right thigh of nude mice (20-25 g; Harlan-Sprague-Dawley) by injecting 1×10^6 viable tumor cells suspended in PBS. When tumors had grown to 4 to 6 mm in average diameter (2 weeks), the mice were randomly allocated into two groups (four mice per group). Mice in group 1 were injected with ^{111}In-DTPA-C225-HAuNS, and mice in group 2 were injected with ^{111}In-DTPA-IgG-HAuNS (both at a dose of $\sim 7.3 \times 10^{10}$ particles/mL, 10 μCi/mouse in 0.13 mL). Mice were killed by CO_2 exposure followed by cervical dislocation 24 h after injection. Blood, heart, liver, spleen, kidney, lung, stomach, intestine, muscle, bone, and tumor tissues were removed and weighed, and radioactivity was measured with a Cobra γ counter (Packard). Uptakes of nanoshells in various organs were calculated as %ID/g.

Half of the tumors that were removed were cryosectioned into 5-μm sections, mounted on slides, fixed in cold acetone for 15 min, washed three times with PBS, and stained with DAPI at room temperature for 5 min. The slides were then examined under a fluorescence microscope equipped with a dark-field condenser to determine the intratumoral distribution of HAuNS in the perivascular area. The slide immediately adjacent to the one stained with DAPI was stained with H&E to confirm the presence of tumors.

Statistical Analysis

Differences in biodistribution data were analyzed using a two-tailed unpaired Student's t test, with $P < 0.05$ considered to be statistically significant.

Results

Synthesis and Characterization of Antibody-HAuNS Conjugates

HAuNS were prepared by the cobalt nanoparticle-mediated reduction of chloroauric acid (18). Antibody was covalently conjugated to the gold surface through sulfhydryl groups introduced to the antibody (Fig. 1). C225 or control IgG antibody was first functionalized with activated ester *N*-succinimidyl *S*-acetylthioacetate to introduce SH-protected *S*-acetylthioacetate groups. The radiometal chelator DTPA was subsequently conjugated to each antibody through an isothiocyanate-mediated coupling reaction. The DTPA-containing antibodies were finally conjugated to the gold surface of HAuNS through the S-Au bond after free SH in the antibody was released by treating DTPA-antibody-ATA with hydroxylamine. Once the antibody had been attached to the HAuNS, complete coverage of the gold surface in HAuNS was ensured by treating the antibody-coated HAuNS with an excess of polyethylene glycol-SH (Fig. 1).

TEM images showed a haze ring around C225-HAuNS, which was not seen in plain HAuNS, confirming coating of HAuNS with the C225 antibody (Fig. 2A). The diameter of the HAuNS, the thickness of the Au shell, and the thickness of the antibody coating were $\sim 30.4 \pm 4.4$, 7.8 ± 2.2, and 3.7 ± 0.8 nm, respectively, as measured from TEM images. The diameter of nanoshells was further determined by dynamic light scattering to be ~ 34.4 nm for plain HAuNS and 37.0 nm for C225-HAuNS, confirming that a layer of antibody molecules of ~ 2.6 to 3.5 nm was coated onto the nanoshells.

The absorbance spectra showed an 18-nm blue shift in the extinction maximum (λ_{max}) of the HAuNS sample after antibody conjugation (Fig. 2B). Antibody-conjugated HAuNS exhibited excellent colloidal stability; no apparent aggregation or change in the UV-visible spectra was observed when the nanoshells were stored in PBS buffer at 4°C over a period of 3 weeks. The HAuNS concentration was calculated from the volume of each nanoshell and from the gold concentration, which was determined by

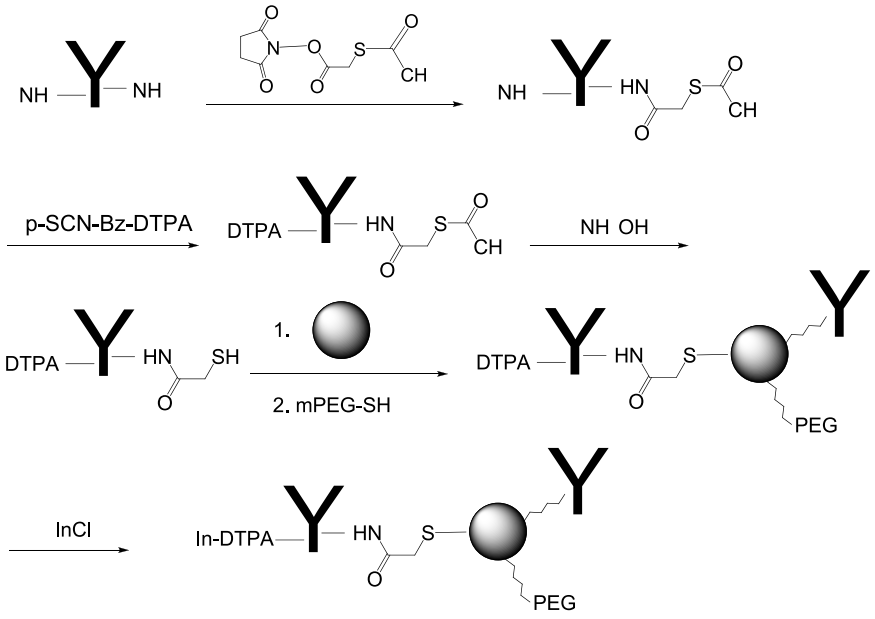

Figure 1. Schema for the synthesis of immuno-HAuNS bioconjugates.

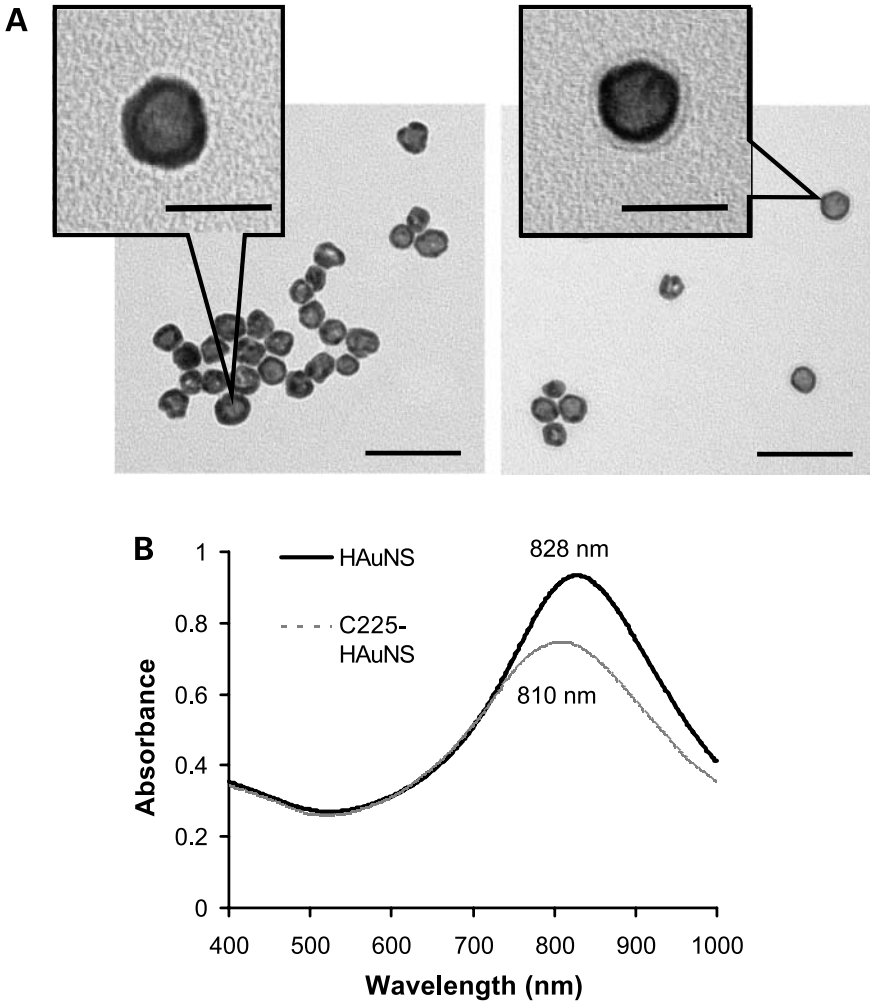

Figure 2. **A,** transmission electron micrographs of the plain HAuNS (*left*) and C225-HAuNS (*right*) reveal the morphology of HAuNS. The images also show the presence of a layer of C225 antibody coating on the shells of HAuNS. **B,** absorption spectra of the HAuNS showing the plasma resonance peak tuned to the NIR region and the blue shift after C225 conjugation. λ_{max} = 828 nm for HAuNS and λ_{max} = 810 nm for C225-HAuNS. Bar, 50 μm.

inductively coupled plasma mass spectroscopic analysis. The nanoshell concentrations were then plotted against the measured absorbance values to yield a nanoparticle extinction coefficient of $\varepsilon = 8.3 \times 10^9$ mol/L^{-1} cm^{-1} (1.37×10^{-11} mL/particle/cm) for the plasma band at 808 nm. This value was used to estimate the concentration of other HAuNS solutions. Each nanoshell particle was estimated to be covered by ~124 antibody molecules as determined by the bicinchoninic acid protein assay.

In vitro Binding of C225-HAuNS to A431 Cells and Photothermal Effect

Figure 3 compares the light-scattering images of A431 cells incubated with C225-HAuNS, IgG-HAuNS, or C225-HAuNS plus a large excess of C225 (blocking). Only dim greenish light was detected when cells were incubated with IgG-HAuNS. This signal was due to autofluorescence and scattered light from the cell organelles in the cell cytoplasm and membrane. In contrast, C225-HAuNS exhibited a strong signal in perinucleic areas in the cells. Moreover, uptake of C225-HAuNS in the A431 cells was efficiently blocked by the anti-EGFR antibody C225 (Fig. 3). The signal intensity from scattered light in cells treated with C225-HAuNS was 10-fold higher than that in cells treated with IgG-HAuNS. Similar scattering intensities were observed when we compared cells exposed to IgG-HAuNS with cells exposed to C225-HAuNS plus C225.

Exposure of aqueous solutions of C225-HAuNS to an 8 W/cm^2 laser caused heating of the solutions. The temperatures in the solutions containing 3.7×10^{10} and 7.3×10^{10} nanoshells/mL increased with increasing exposure time and reached plateaus at 34.8°C and 41.5°C after ~4 min of light exposure, representing elevations of 9.8°C and 16.5°C, respectively (Fig. 4A). Without HAuNS, little temperature change was observed. These data indicate that C225-HAuNS acted as an efficient photothermal coupling agent.

Twenty-four hours after laser treatment, most A431 cells treated with C225-HAuNS followed by NIR laser irradiation (40 W/cm^2 for 5 min) were dead (lysed or stained red with EthD-1); none of the other groups (control, C225-HAuNS alone, irradiation alone, and IgG-HAuNS plus laser) showed observable damage to the cancer cells (Fig. 4B). Morphologically, viable A431 cells were polygonal without treatment. Few cells were stained red with

EthD-1. After treatment with C225-HAuNS plus laser, most cells were lysed. The remaining few cells stained positive with calcein (green) were more rounded possibly as a result of condensation of skeleton proteins (*asterisk* in Fig. 4C). Some of the cells that were stained positive with EthD-1 24 h after laser treatment had already lost cellular integrity (*arrow* in Fig. 4C).

In vivo Biodistribution

To enable quantitative analysis, HAuNS nanoparticles were labeled with the γ emitter ^{111}In, which has a desirable physical half-life ($t_{1/2}$ = 67.3 h). Radiolabeling of the nanoparticles was accomplished through incubation of $^{111}InCl_3$ with DTPA-antibody-HAuNS conjugates in sodium acetate buffer at pH 5.5 and room temperature. Unlabeled ^{111}In and ^{111}In-DTPA-antibody were removed by centrifugation and washing steps. The radiochemical purities for both ^{111}In-DTPA-C225-HAuNS and ^{111}In-DTPA-IgG-HAuNS were >95%.

The biodistribution of ^{111}In-labeled antibody-HAuNS at 24 h after injection is presented in Fig. 5. The organs that had the highest uptakes of both ^{111}In-labeled C225-HAuNS and IgG-HAuNS were the liver (33.07 ± 3.40%ID/g versus 13.20 ± 2.51%ID/g), the spleen (17.49 ± 4.55%ID/g versus 17.69 ± 4.05%ID/g), and the kidney (13.63 ± 1.98%ID/g versus 14.80 ± 4.90%ID/g). ^{111}In-labeled C225-HAuNS had significantly higher uptake in the liver than did ^{111}In-labeled IgG-HAuNS (P = 0.001). In the tumor, ^{111}In-labeled C225-HAuNS showed a higher uptake value (6.81 ± 2.64%ID/g) than ^{111}In-labeled IgG-HAuNS (4.60 ± 1.31%ID/g), although the difference was not statistically significant (P = 0.089; Fig. 5). The tumor uptake of nanoparticles was further analyzed by counting the number of nanoshells per observation field in the perivascular area. The uptake of C225-HAuNS in the tumor was significantly greater than that of IgG-HAuNS (Fig. 6). The average nanoshell counts per field at ×200 magnification were 56.6 ± 9.1 in tumors of mice injected with C225-HAuNS and 15.8 ± 6.0 in tumors of mice injected with IgG-HAuNS (P = 0.003).

Discussion

Tunable gold nanoparticles designed to have strong NIR absorption can serve as photothermal coupling agents to mediate localized heating of the target tissues. The further development of this therapeutic strategy in oncology requires the broader availability of a variety of bioconjugated

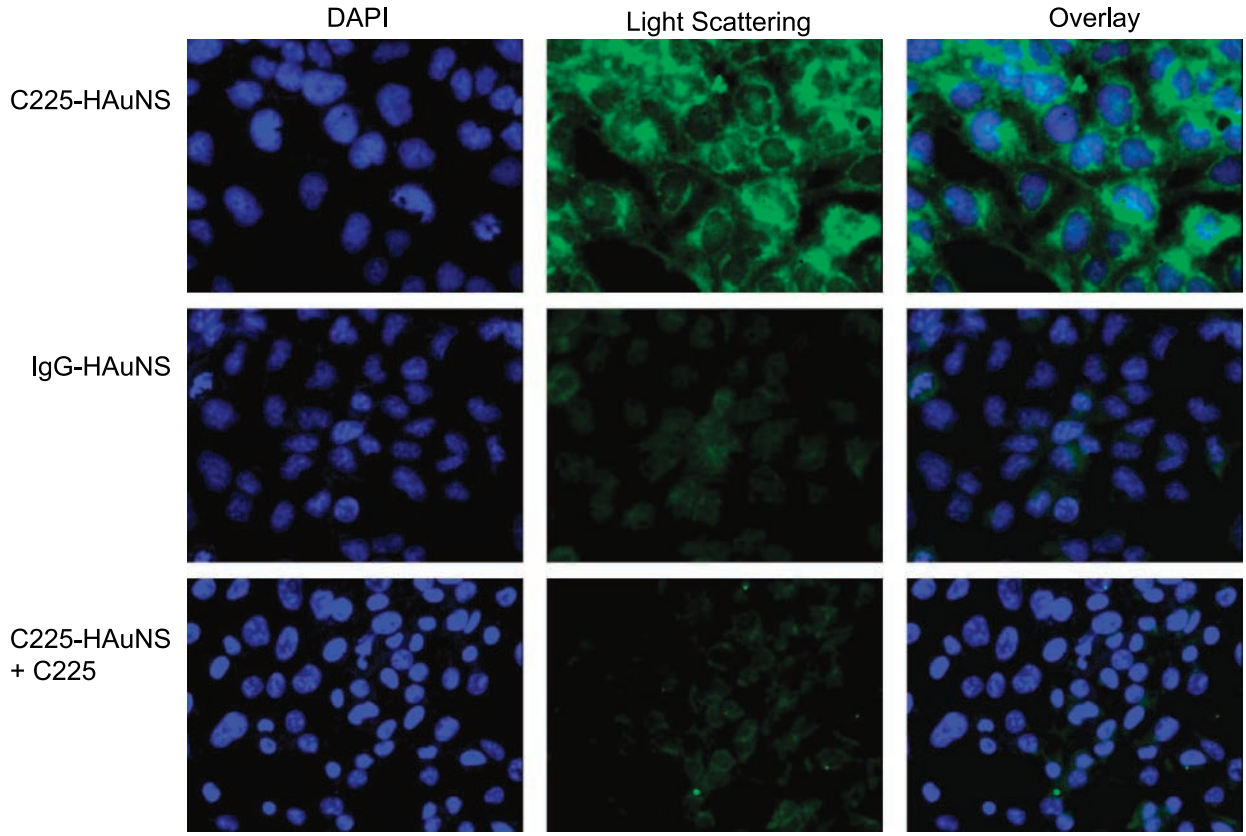

Figure 3. Selective binding of anti-EGFR-conjugated HAuNS to A431 cells. A431 cells were seeded onto a 96-well plate and incubated with C225-HAuNS (7.3×10^{10} particles/mL), IgG-HAuNS (7.3×10^{10} particles/mL), or C225 (500 μg/mL) plus C225-HAuNS for 30 min at 37°C. Only cells incubated with C225-HAuNS had a strong light-scattering signal. Cells were stained with DAPI for visualization of cell nuclei (*blue*). Light-scattering images of nanoshells were pseudocolored green. Original magnification, ×630.

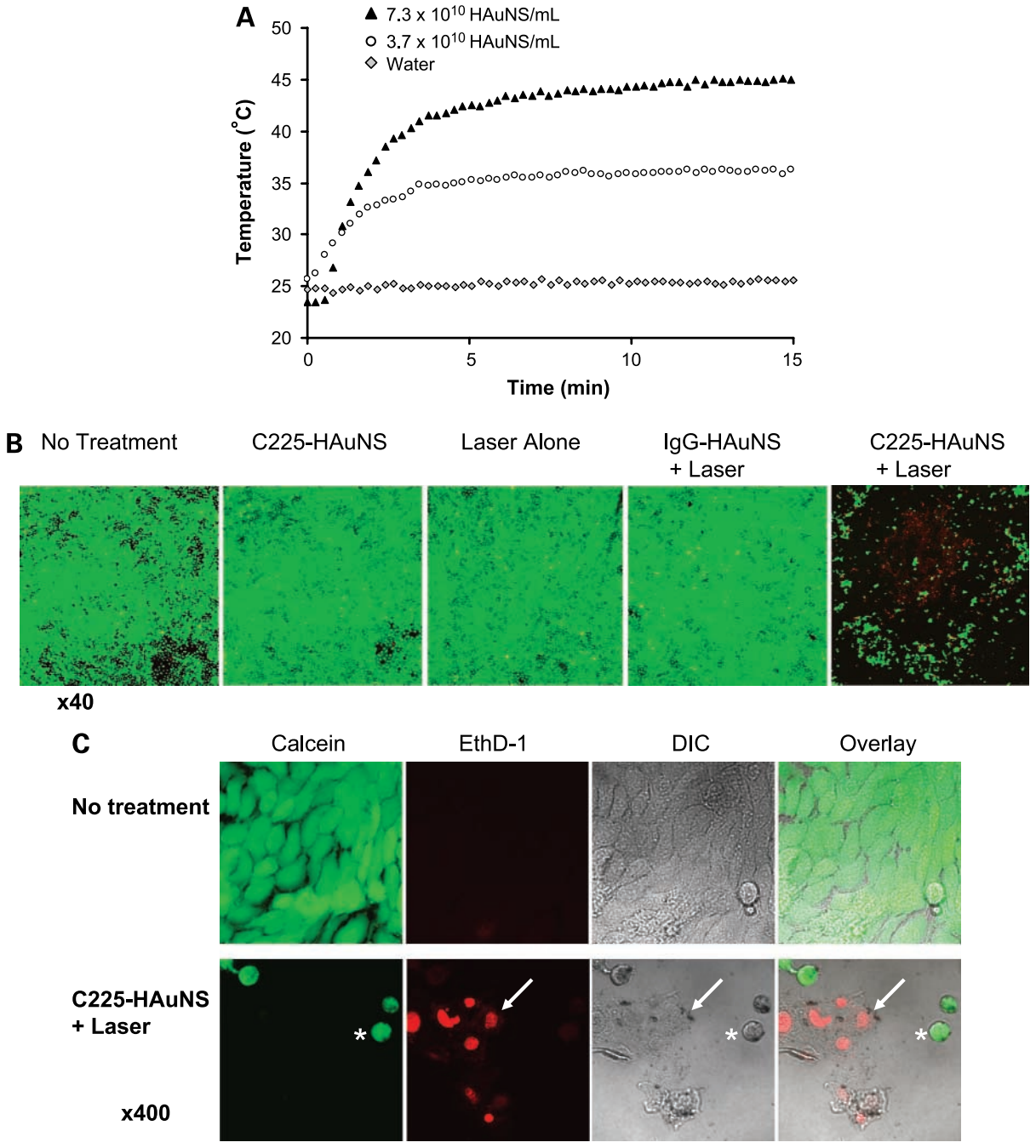

Figure 4. **A,** heating of aqueous C225-HAuNS solutions exposed to NIR light centered at 808 nm at 8 W/cm^2. **B,** cell viability after various treatments. Cells retained normal morphology with no apparent death observed (stained green with calcein CM) when cells were not treated or treated with C225-HAuNS alone, NIR laser alone, or nontargeted IgG-HAuNS plus NIR laser. In contrast, most cells were dead after treatment with C225-HAuNS plus NIR laser. Dead cells were labeled red with EthD-1. Magnification, ×40. **C,** images of untreated viable cells and dead cells treated with C225-HAuNS and NIR laser at higher magnification (×400). The dead cells showed rounded morphology (*asterisk*) and membrane damage as indicated by positive staining with EthD-1 (*arrow, red*). *DIC,* differential interference contrast.

gold nanoparticles tuned to NIR for selective tumor destruction. In this study, we synthesized and characterized immuno-HAuNS conjugates targeted to EGFR and showed the selective photothermal killing of cancer cells *in vitro* as well as increased uptake *in vivo* in A431 tumors that overexpress EGFR. The following features make the current design particularly attractive. First, the nanoshell used here was a HAuNS made up of only gold, with the silica core eliminated. This is more advantageous because of the concern of potential cytotoxicity of silica in

silica-cored nanoshells. Secondly, photothermal therapies may benefit from the small size of HAuNS in terms of their ability to permeate tumor blood vessels. The HAuNS used in the current study, which had a diameter of ~30 nm, should have a better chance to extravasate and to achieve targeted delivery than much larger silica-cored nanoshells (diameter, >110 nm; refs. 24, 25). Spheres with a diameter of ~30 nm are also optimal for intracellular uptake by mammalian cells as shown recently (26). Apart from these inherent properties, HAuNS as prepared could be readily stabilized with antibodies. This is different from gold nanorods, which use cetyltrimethylammonium bromide surfactant to stabilize the nanorod solutions. Biological applications of gold nanorods have not been widely pursued partly because of the presence of cetyltrimethylammonium bromide surfactant (17, 27). Cetyltrimethylammonium bromide released from nanorods is cytotoxic, and attempting to remove the bulk cetyltrimethylammonium bromide from nanorods would cause particle aggregation (28).

Previously, immuno-gold nanoparticles have been prepared by electrostatic interactions (29, 30). Loo et al. (10) tethered antibody to nanoshells through a polyethylene glycol chain. In the present work, antibody was conjugated to HAuNS through gold thiol bonds, enabling the formation of stable immuno-AuNS. Sulfhydryl functional groups in the antibody were introduced by reacting antibody with *N*-succinimidyl *S*-acetylthioacetate followed by activation and releasing of free SH by treatment with hydroxylamine (Fig. 1). TEM images of the immuno-HAuNS showed a haze around the HAuNS, which did not exist in plain HAuNS, confirming coating of an antibody layer on the nanoshells (Fig. 2A). The extinction spectra displayed in Fig. 2B provided further evidence that the antibody layer had been coated onto the HAuNS. On C225 antibody coating, the spectra showed a shift in the plasma resonance peak wavelength of 18 nm and a decrease of ~20% in absorbance. The shift in the absorption peak is possibly due to the altered refractive index of the local environment of the nanoparticle caused by the presence of the biological molecules (31). Reduced absorbance may be caused by loss of C225-HAuNS during gel chromatography purification, scattering of light by the antibody coating layer, and/or the formation of aggregates. Because little further reduction of the immuno-HAuNS absorbance peak was seen within 3 weeks in storage, it is unlikely that the initial reduction in peak absorbance observed with C225-HAuNS was due to aggregation.

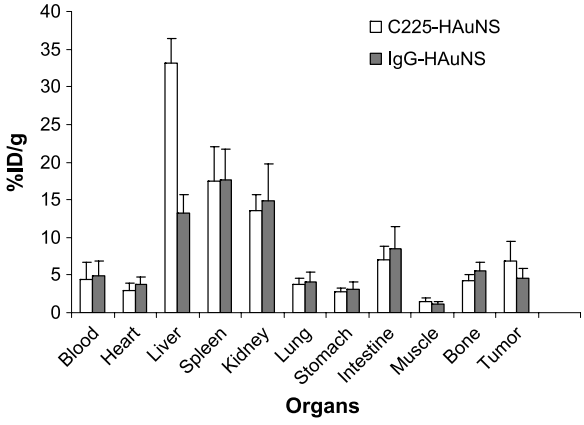

Figure 5. Biodistribution of ^{111}In-labeled DTPA-C225-HAuNS and DTPA-IgG-HAuNS. Uptake in the liver was significantly higher with ^{111}In-DTPA-C225-HAuNS than with ^{111}In-DTPA-IgG-HAuNS (P = 0.001). Tumor uptake was higher with ^{111}In-DTPA-C225-HAuNS than with ^{111}In-DTPA-IgG-HAuNS, but the difference was not statistically significant (P = 0.08). Mean ± SD %ID/g (n = 4).

Quantitative analysis of antibodies on the surface of nanoshells is challenging. Using the bicinchoninic acid protein assay, we estimated the amount of C225 attached to the HAuNS to be 124 antibodies/nanoshell. The amount of antibody that would form a monolayer on the surface of HAuNS could be calculated using saturation capacity data of ~2.5 mg/m^2 for IgG (or ~100 nm^2/antibody) provided by Cantarero et al. (32). Thus, based on the spherical shape and radius of 15 nm, the number of antibodies on the gold surface was 28 antibodies/nanoshell calculated by dividing the total surface area of a nanoshell by the head group surface area of an antibody. The value obtained with the protein assay is 4.4 times greater than that estimated by theoretical calculation. One possible explanation is that the measured protein concentration may be affected by the presence of nanoshells and vice versa (33). The bicinchoninic acid method measures protein concentration at 562 nm. Nanoshells had significant extinction at 562 nm. Although the contribution of nanoshells was removed by simple subtraction of the spectrum of pure nanoshells at the same concentration as the immuno-nanoshells, this subtraction ignores potential NIR enhancements of the bicinchoninic acid spectrum. In spite of the inaccuracy in quantifying antibodies attached to the surface of HAuNS, the large measured stoichiometry suggests that a significant portion of the immuno-HAuNS contains antibodies.

Selective photothermal destruction of cancer cells mediated by HAuNS requires specific binding of the nanoshells to the target cells. As shown in Fig. 3, C225-HAuNS but not IgG-HAuNS bound to A431 cells overexpressing EGFR. Moreover, the uptake of C225-HAuNS to A431 cells could be completely blocked by C225, indicating that C225-HAuNS was taken up by the A431 cells via EGFR-mediated endocytosis. Further experiments showed that exposure of an aqueous solution containing immuno-HAuNS (7.3×10^{10} nanoshells/mL) to NIR laser resulted in a rapidly elevation of temperature up to 16.5°C (Fig. 4A). Such an effect is comparable with that achieved with AuNS containing a superparamagnetic iron oxide-silica core but at a much higher AuNS concentration (7.5×10^{12} nanoshells/mL; ref. 34). These data indicate that immuno-HAuNS could act as an efficient photothermal coupling agent.

After NIR laser exposure of 40 W/cm^2 for 5 min, almost all A431 cells treated with C225-HAuNS within the laser spot were destroyed, an effect that was not observed in cells exposed to C225-HAuNS alone, NIR laser alone, or

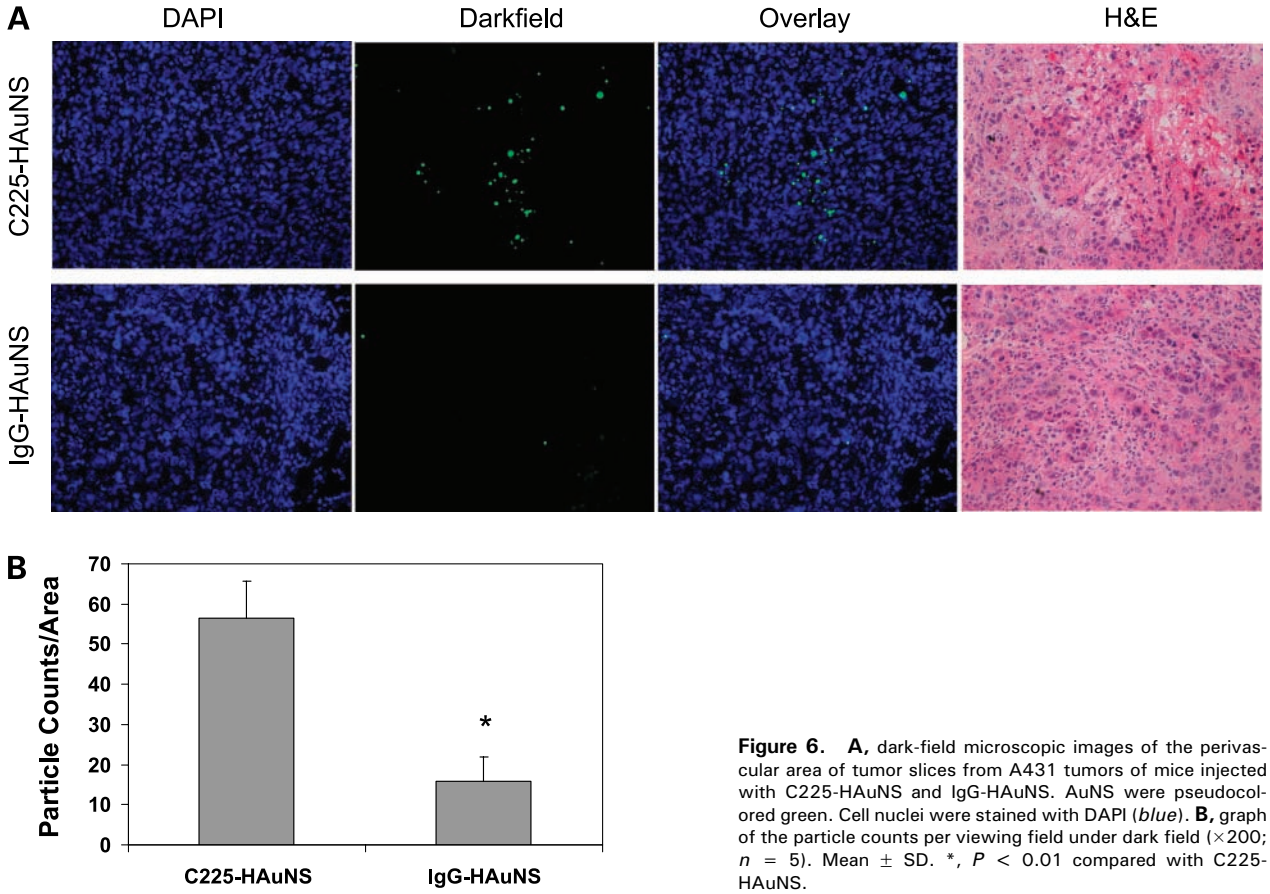

Figure 6. **A,** dark-field microscopic images of the perivascular area of tumor slices from A431 tumors of mice injected with C225-HAuNS and IgG-HAuNS. AuNS were pseudocolored green. Cell nuclei were stained with DAPI (*blue*). **B,** graph of the particle counts per viewing field under dark field (×200; $n = 5$). Mean ± SD. *, $P < 0.01$ compared with C225-HAuNS.

nonspecific IgG-HAuNS plus NIR laser. Evidence of irreversible cell membrane damage was noted via imaging of the EthD-1, which is normally impermeable to healthy cells. The dye was found in the intracellular space of cells exposed to both C225-HAuNS and the laser but was not observed in control cells that received the various other treatments (Fig. 4B and C). Extensive cell heating caused by continuous NIR absorption mediated by C225-HAuNS was the most likely origin of cell death. These data indicate that the laser at output power of 40 W/cm^2 was safe to use and that it is possible to selectively induce photothermal destruction of EGFR-positive cells with HAuNS targeted to EGFR.

For active targeting approaches to work *in vivo*, it is imperative that AuNS are capable of extravasating into the interstitial space. In this context, nanoparticles with smaller diameters are expected to be more effective for extravasation into tumor than particles of larger sizes. In addition to size consideration, the lack of a quantitative method to determine the gold nanoparticle content in tissues also impeded the evaluation of *in vivo* targeting efficiency of AuNS. In the current study, ^{111}In-labeled immuno-HAuNS was used to monitor the tissue distribution of HAuNS after i.v. injection. C225-HAuNS showed significantly higher uptake in the liver than did IgG-HAuNS (Fig. 5). Liver is known to express a high level of EGFR (35, 36), which would explain the significantly higher level of liver uptake of C225-HAuNS compared with IgG-HAuNS. Radiotracer counting study also showed that C225-HAuNS had a higher uptake value in the A431 tumors than did IgG-HAuNS, representing a 48% gain for targeted HAuNS. Significantly, there was >3-fold increase in the number of nanoshells and/or nanoshell aggregates per field observed under dark-field microscope in the perivascular area of the tumor in mice injected with C225-HAuNS than in mice injected with IgG-HAuNS (Fig. 6), suggesting that the interaction between C225-HAuNS and EGFR may have facilitated extravasation of the nanoshells into the interstitial space. However, in areas away from the tumor vasculature, neither C225-HAuNS nor IgG-HAuNS was often seen. This may be caused by limited diffusion of nanoparticles in interstitial space after successful transvascular transport. Alternatively, it is plausible that the ''binding-site barrier,'' by which the extravascular transport of nanoparticle is prevented because of strong initial binding of nanoparticles to their target, may have caused dispersion of immuno-HAuNS in tumor matrix (37). Further improvement in the delivery of targeted HAuNS will require a careful design of nanoshells with increased efficiency in extravasation from tumor vessels and distribution into interstitial space away from the perivascular area.

Conclusions

Immuno-HAuNS targeted to EGFR have been shown to selectively bind to EGFR-positive cells and destroy these cells via a photothermal effect. *In vivo* tissue distribution and *ex vivo* analysis of scattered light from nanoshells showed increased tumor uptake of targeted immuno-HAuNS to tumors expressing EGFR mainly to the perivascular area of the tumor. Up to 6.8%ID/g was taken up by the tumor with C225-HAuNS. Because of the favorable physicochemical properties of HAuNS (30 nm average diameter; no silica core), targeted HAuNS may find increasing applications in photothermal ablation therapy. *In vivo* photothermal ablation studies showing increased treatment efficacy with C225-HAuNS are currently under way.

Disclosure of Potential Conflicts of Interest

No potential conflicts of interest were disclosed.

Acknowledgments

We thank Michael Worley for editing the article and Kenneth Dunner for assistance and use of the TEM facility, which was supported by the Cancer Center Core Grant CA16672 to The University of Texas M. D. Anderson Cancer Center.

References

1. Fiedler VU, Schwarzmaier HJ, Eickmeyer F, et al. Laser-induced interstitial thermotherapy of liver metastases in an interventional 0.5 Tesla MRI system: technique and first clinical experiences. J Magn Reson Imaging 2001;13:729 – 37.

2. Vogel A, Venugopalan V. Mechanisms of pulsed laser ablation of biological tissues. Chem Rev 2003;103:577 – 644.

3. Lapotko D, Lukianova E, Potapnev M, Aleinikova O, Oraevsky A. Method of laser activated nano-thermolysis for elimination of tumor cells. Cancer Lett 2006;239:36 – 45.

4. Vogl TJ, Straub R, Eichler K, Sollner O, Mack MG. Colorectal carcinoma metastases in liver: laser-induced interstitial thermotherapy-local tumor control rate and survival data. Radiology 2004;230:450 – 8.

5. Curley SA, Izzo F, Delrio P, et al. Radiofrequency ablation of unresectable primary and metastatic hepatic malignancies: results in 123 patients. Ann Surg 1999;230:1 – 8.

6. Seki T, Wakabayashi M, Nakagawa T, et al. Ultrasonically guided percutaneous microwave coagulation therapy for small hepatocellular carcinoma. Cancer 1994;74:817 – 25.

7. Jolesz FA, Hynynen K, McDannold N, Freundlich D, Kopelman D. Noninvasive thermal ablation of hepatocellular carcinoma by using magnetic resonance imaging-guided focused ultrasound. Gastroenterology 2004;127:S242 – 7.

8. Liapi E, Geschwind J-FH. Transcatheter and ablative therapeutic approaches for solid malignancies. J Clin Oncol 2007;25:978 – 86.

9. Hirsch LR, Stafford RJ, Bankson JA, et al. Nanoshell-mediated near-infrared thermal therapy of tumors under magnetic resonance guidance. Proc Natl Acad Sci U S A 2003;100:13549 – 54.

10. Loo C, Lin A, Hirsch L, et al. Nanoshell-enabled photonics-based imaging and therapy of cancer. Technol Cancer Res Treat 2004;3:33 – 40.

11. Weissleder R. A clearer vision for *in vivo* imaging. Nat Biotechnol 2001;19:316 – 7.

12. O'Neal DP, Hirsch LR, Halas NJ, Payne JD, West JL. Photo-thermal tumor ablation in mice using near infrared-absorbing nanoparticles. Cancer Lett 2004;209:171 – 6.

13. Matsumura Y, Maeda H. A new concept for macromolecular therapeutics in cancer chemotherapy: mechanism of tumoritropic accumulation of proteins and the antitumor agent SMANCS. Cancer Res 1986; 46:6387 – 92.

14. Loo C, Lowery A, Halas N, West J, Drezek R. Immunotargeted nanoshells for integrated cancer imaging and therapy. Nano Lett 2005;5: 709 – 11.

15. Chen J, Wang D, Xi J, et al. Immuno gold nanocages with tailored optical properties for targeted photothermal destruction of cancer cells. Nano Lett 2007;7:1318 – 22.

16. El-Sayed IH, Huang X, El-Sayed MA. Selective laser photo-thermal therapy of epithelial carcinoma using anti-EGFR antibody conjugated gold nanoparticles. Cancer Lett 2006;239:129 – 35.

17. Huang X, El-Sayed IH, Qian W, El-Sayed MA. Cancer cell imaging and photothermal therapy in the near-infrared region by using gold nanorods. J Am Chem Soc 2006;128:2115 – 20.

18. Schwartzberg AM, Olson TY, Talley CE, Zhang JZ. Synthesis, characterization, and tunable optical properties of hollow gold nanospheres. J Phys Chem B 2006;110:19935 – 44.

19. Yasui W, Sumiyoshi H, Hata J, et al. Expression of epidermal growth factor receptor in human gastric and colonic carcinomas. Cancer Res 1988;48:137 – 41.

20. Costa S, Stamm H, Almendral A, et al. Predictive value of EGF receptor in breast cancer. Lancet 1988;2:1258.

21. Ang KK, Berkey BA, Tu X, et al. Impact of epidermal growth factor receptor expression on survival and pattern of relapse in patients with advanced head and neck carcinoma. Cancer Res 2002;62:7350 – 6.

22. Mendelsohn J. Epidermal growth factor receptor inhibition by a monoclonal antibody as anticancer therapy. Clin Cancer Res 1997;3: 2703 – 7.

23. Goldstein NI, Prewett M, Zuklys K, Rockwell P, Mendelsohn J. Biological efficacy of a chimeric antibody to the epidermal growth factor receptor in a human tumor xenograft model. Clin Cancer Res 1995;1: 1311 – 8.

24. Kong G, Braun RD, Dewhirst MW. Hyperthermia enables tumor-specific nanoparticle delivery: effect of particle size. Cancer Res 2000;60: 4440 – 5.

25. Yang Z, Zheng S, Harrison WJ, et al. Long-circulating near-infrared fluorescence core-cross-linked polymeric micelles: synthesis, characterization, and dual nuclear/optical imaging. Biomacromolecules 2007;8: 3422 – 8.

26. Chithrani BD, Ghazani AA, Chan WC. Determining the size and shape dependence of gold nanoparticle uptake into mammalian cells. Nano Lett 2006;6:662 – 8.

27. Sims-Mourtada J, Izzo JG, Apisarnthanarax S, et al. Hedgehog: an attribute to tumor regrowth after chemoradiotherapy and a target to improve radiation response. Clin Cancer Res 2006;12:6565 – 72.

28. Connor EE, Mwamuka J, Gole A, Murphy CJ, Wyatt MD. Gold nanoparticles are taken up by human cells but do not cause acute cytotoxicity. Small 2005;1:325 – 327.

29. Sokolov K, Follen M, Aaron J, et al. Real-time vital optical imaging of precancer using anti-epidermal growth factor receptor antibodies conjugated to gold nanoparticles. Cancer Res 2003;63:1999 – 2004.

30. El-Sayed IH, Huang X, El-Sayed MA. Surface plasmon resonance scattering and absorption of anti-EGFR antibody conjugated gold nanoparticles in cancer diagnostics: applications in oral cancer. Nano Lett 2005;5:829 – 34.

31. Haes AJ, Chang L, Klein WL, Van Duyne RP. Detection of a biomarker for Alzheimer's disease from synthetic and clinical samples using a nanoscale optical biosensor. J Am Chem Soc 2005;127:2264 – 71.

32. Cantarero LA, Butler JE, Osborne JW. The adsorptive characteristics of proteins for polystyrene and their significance in solid-phase immunoassays. Anal Biochem 1980;105:375 – 82.

33. Calabretta M, Jamison JA, Falkner JC, et al. Analytical ultracentrifugation for characterizing nanocrystals and their bioconjugates. Nano Lett 2005;5:963 – 7.

34. Ji X-J, Shao R-P, Elliott AM, et al. Bifunctional gold nanoshells with a superparamagnetic iron oxide core suitable for both MR imaging and photo-thermal therapy. J Phys Chem C 2007;111:6245 – 51.

35. Divgi CR, Welt S, Kris M, et al. Phase I and imaging trial of indium 111-labeled anti-epidermal growth factor receptor monoclonal antibody 225 in patients with squamous cell lung carcinoma. J Natl Cancer Inst 1991;83:97 – 104.

36. Mulkern RV, Panych LP, McDannold NJ, Jolesz FA, Hynynen K. Tissue temperature monitoring with multiple gradient-echo imaging sequences. J Magn Reson Imaging 1998;8:493 – 502.

37. Adams GP, Schier R, McCall AM, et al. High affinity restricts the localization and tumor penetration of single-chain Fv antibody molecules. Cancer Res 2001;61:4750 – 5.